The role of sulphur in the early production of copper red stained glass

Mingyue Yuan, Jordi Bonet, Marine Cotte, Nadine Schibille, Bernard Gratuze, Trinitat Pradell

Ceramics International xxx (xxxx) xxx

Contents lists available at ScienceDirect

Ceramics International

journal homepage: www.elsevier.com/locate/ceramint

The role of sulphur in the early production of copper red stained glass

Mingyue Yuan [a], Jordi Bonet [b], Marine Cotte [c,d], Nadine Schibille [e], Bernard Gratuze [e], Trinitat Pradell [a,*]

[a] Physics Department and Barcelona Research Centre in Multiscale Science and Engineering, Universitat Politècnica de Catalunya, BarcelonaTech, Campus Diagonal Besòs, c) Av. Eduard Maristany 16, 08930, Barcelona, Spain
[b] J.M. Bonet Vitralls S.L, c) Corominas 17, 08902, L'Hospitalet de Llobregat, Barcelona, Spain
[c] ESRF, The European Synchrotron, CS 40220, 38043 Grenoble Cedex 9, France
[d] Laboratoire d'Archéologie Moléculaire et Structurale(LAMS), CNRS, UMR 8220, Sorbonne Université, UPMC Univ. Paris 06, 4 Place Jussieu, 75005, Paris, France
[e] Institut de Recherche sur les Archéomatériaux(IRAMAT), UMR 7065, CNRS/Université d'Orléans, Centre Ernest Babelon, Orléans, France

ARTICLE INFO

Handling Editor: Dr P. Vincenzini

Keywords:
Glass
Sulphide-silicate partition melt
Copper nanoparticles
Copper sulphide
Micro-X-ray absorption spectroscopy

ABSTRACT

Little is known about the production of ruby red copper stained glasses from the Medieval and Renaissance periods apart from the fact that the colour is due to the presence of small metallic copper nanoparticles and that tin, the most common reducing agent used in copper red glass production since the 19th century, is not present. In fact, very few workshops in Europe were able to make red glass in historical times, and they kept it secret, so very little is known about how it was obtained. These workshops exported the red glass throughout Europe. Recently, the presence of copper sulphide particles and the data obtained in the replication red glass following historical recipes suggested that sulphur might be the key ingredient in this process.

Here, a collection of historical red glasses from these periods has been analysed using a combination of microanalytical techniques; Electron Microprobe (EM) and Field Emission and Scanning Electron Microscopy (FESEM) to verify the chemical composition and nanostructure of the glasses, Synchrotron radiation micro-X-Ray Diffraction (micro-XRD) to establish the nature of the nanocrystalline precipitates, and S, Cu and Fe K-edge micro-X-Ray Absorption Spectroscopy (micro-XAS) to determine the speciation. The data obtained show that the oxidation of S^{2-} into S^{6+} in the glass is responsible for the precipitation of copper nanoparticles. The development of a sulphide-silicate partition and the presence of Fe^{3+} in the melt give rise to the precipitation of the high-pressure tetragonal polymorph of chalcocite (Cu_2S). Differences between the Medieval and Renaissance red glass are determined.

1. Introduction

Red glasses were used in stained-glass windows in Europe since medieval times. In fact, the production of transparent red glass was a medieval European achievement, as earlier red glasses were typically opaque [1]. The ruby red colouring shown by the glasses is due to the presence of metallic copper nanoparticles [2–8]. Very small particles, typical sizes below 50 nm, are required, as larger precipitates impart a livery red colour to the glass and scatter light, increasing opacity [9,10]. A very low fraction of particles (between 0.02% and 0.05% volume fraction) is also mandatory, as the absorption and scattering of light by the particles drastically reduce the transparency of the glasses. For this reason, historical red stained glasses were obtained by applying one or several thin layers of red glass over a thick colourless transparent base glass. Different types have been identified [7,8,11]; *striated* glass refers to a glass made of multiple alternating thin layers of red and clear glass, *sandwich* glass describes a single layer of red glass covered with a layer of clear glass and *flashed* glass is a single layer of red glass applied over the thick clear base glass. *Striated* glass dates mainly to the 12th and 13th century, *sandwich* since the 13th century, and the *flashed* glass, which is the only surviving glass, from the 17th century.

Stained red glasses are blown glasses, that is, a molten glass is gathered on an iron cane and blown into a cylinder which is afterwards cut and flattened while hot. To obtain a thin red glass layer, in modern times the molten clear base glass is coated with red glass and blown together.

The solubility of metallic copper in a silicate melt is very low and the equilibrium of copper species includes Cu^{+} and Cu^{2+}. Some glasses show

* Corresponding author.
E-mail address: Trinitat.Pradell@upc.edu (T. Pradell).

https://doi.org/10.1016/j.ceramint.2023.02.236
Received 20 December 2022; Received in revised form 20 February 2023; Accepted 27 February 2023
Available online 1 March 2023

a higher solubility for metallic copper than others; for instance, adding Pb^{2+} to the glass is known to enhance the solubility of metallic copper. However, in any case, the melt incorporates copper mainly in its oxidised forms. As the ruby red colour is rendered by the formation of metallic copper nanoparticles, at some point the glass has to be reduced to induce their precipitation avoiding the precipitation of other copper compounds such as cuprite (Cu_2O) or the development of large Cu^o particles (livery red). The use of a reducing atmosphere or the introduction of reducing agents in the melt is commonly used to render the precipitation of the copper nanoparticles. Modern red glass is obtained by adding lead, tin and iron; lead and tin increase the solubility of copper in the glass and tin and iron act as reducing agents [2,3,12]. The presence of tin and iron is documented in red copper *flashed* glasses since the mid of the 17th century. However, with regard to Medieval and Renaissance stained glasses, tin is present only in trace amounts and iron is present in lower amounts than in later glasses [8,13].

Very few workshops in Europe were able to make red glass in historical times, and they kept it secret, so very little is known about how it was obtained. These workshops exported the red glass throughout Europe.

Some analysis of red stained glasses from the Medieval period have been carried out to understand the mechanisms involved in their production [7,8,14]. Broadly speaking, the reduction of copper to the metallic state was associated with the oxidation of iron during the firing of the glass. For the *striated* glass, a mechanism involving the precipitation of the copper metallic nanoparticles at the interphase between intermixed copper rich oxidised and copper-free reduced glass layers has been proposed [7,8]. However, considering the greater thickness (about 200 μm) and homogeneity shown by the red layers in the *sandwich* and *flashed* red glasses, this process is not very likely.

Some information is also obtained from historical documents. The production of stained glass is first described in the manuscript *De diversis artibus* (1090–1125) by the German monk Theophilus [5,15]. Very little is said about coloured glasses and nothing about red glasses. However, this is not until the 17th c. when the decrease in the production of coloured glass and the fear of loss of knowledge resulted in the proliferation of several treatises among them the manuscript *L'art vetraria* by Neri (1612) [16] and later the *Ars Vitraria Experimentalis* (1679) by Kunckel [17].

Recently several attempts have been made to replicate the method of production described in these treatises. Besides the incongruency between the chemical composition of the glasses obtained compared to the historical glasses, red glass has been replicated following several recipes described in Kunkel's treatise [18]. The main conclusions of the study indicate that the incorporation of sulphur seemed fundamental to attain the red colour and that an adequate control of the temperature (above 1100°C) was more important than controlling the furnace atmosphere.

This study was rendered by our observation of the presence of copper sulphide precipitates in some *sandwich* red glasses dated to the Medieval (13th −14th c.) and Renaissance (15th and 16th c.) periods. This has suggested that the presence of sulphur had an important role in the formation of metallic copper nanoparticles in agreement with the work of Vilarigues [18]. However, the role of sulphur in the precipitation of metallic copper nanoparticles has not yet been studied, nor its connection with the role of iron previously sustained by some studies [14]. For this reason, a collection of red glasses, all of them of *sandwich* type, expanding from the 13th c. to the 16th c. mainly from Catalonia together with a piece of 16th c. red glass of Flemish origin belonging to the cathedral of Segovia have been gathered and analysed. Local stained glass was produced in Catalonia since the Romanesque period but red glasses were imported from central Europe [19,20]. Evidence of imported red glass from specialised workshops has also been determined in Italy, Spain and the UK [8].

Using a combination of microanalytical techniques (Electron Microprobe, SEM-FIB-EDS, micro-XRD and micro-XAFS) the composition of the glasses, the nature of the particles and the oxidation state of copper, iron and sulphur were established. Thanks to the micrometric size of the analytical techniques chosen, the mechanisms involved in the production of red glasses in the period were determined and the role of sulphur and iron in the precipitation of the metallic copper nanoparticles was disclosed. Our study has unveiled the mechanisms involved in the development of the red colour in the Medieval and Renaissance. The data has shown a completely different production technique compared to the previous red *striated* and later modern red glasses. Some differences between the Medieval and Renaissance glasses are also identified.

2. Materials and experimental methods

A collection of red glasses from the Medieval and Renaissance periods (13th −16th century) are studied, details shown in Table 1. The collection includes mainly red glasses found in Catalonia. The earliest stained glass known in Catalonia dates to the 11th c. (Museu d'Historia de la Ciutat, Barcelona), the earliest *in-situ* figurative windows to the Monastery of Santes Creus (c. 1200) and some recent discoveries of some panels at the cathedral of Girona. However the collection studied herewith includes the Royal window from the Monastery of Santes Creus (Tarragona) dated c. 1284–1320 [21] and one fragment from a 16th c. restoration from the same place, eight samples belonging to the cathedral of Barcelona; three samples from the Santa Eulalia window dated 1330 of unknown authorship, three samples from the Sant Silvestre window dated 1386 also of unknown authorship, maybe rearranged by Nicoli de Maraye and two samples from Sant Andreu & Sant Llorenç window dated 1398–1408 made by Nicoli de Maraye [22]. One sample from the church of Sant Joan Baptiste at Valls belonging to the rose window made by Giacomo Carnobali (1609) [23] and restored in the 17th c. reusing earlier glass fragments. To complete the collection, a fragment of red glass from the cathedral of Segovia, belonging to the panel glasses made by the Flemish master glaziers Pierres d'Hollande and Pierres de and Pierres de Chiverry between 1544 and 1548, was added.

Cross sections of the samples were embedded in epoxy resin and polished down to 1 μm grade with a diamond paste. The polished sections were examined in reflected and transmitted light with an optical microscope (OM) Nikon Eclipse LV100D equipped with a camera Infinity 1.3C.

The cross sections were coated with a carbon layer (<20 μm thick) and were examined in a crossbeam workstation (Zeiss Neon 40)

Table 1
Details on the samples studied.

sample	dating	original location/ collection	window/artist	glass type
SC13	1284–1320	Monastery of Santes Creus. Tarragona	Royal window/ attributed to Pere d'Insa	sandwich
CB8, CB9, CB10	1330	Cathedral. Barcelona	Santa Eulalia window unknown authorship	sandwich
CB3, CB4, CB5	1386	Cathedral. Barcelona	Sant Silvestre window Rearranged by Nicoli de Maraye	sandwich
CB1, CB2	1398–1408	Cathedral. Barcelona	Sant Andreu & Sant Llorenç window Nicoli de Maraye	sandwich
PS15	1544–1548	Cathedral. Segovia	Pierres d'Hollande & Pierres de Chiverri	sandwich
SC14	1560	Monastery of Santes Creus. Tarragona	Fragment from a 16th c. restoration	sandwich
Valls	1609	Church of Sant Joan Baptiste. Valls	Rose window/Giacomo Carnobali Restauration using old glass fragments	sandwich

equipped with scanning electron microscopy (SEM) GEMINI (Shottky FE) column with attached EDS (Ultim EDS Detector, Oxford Instruments. Aztec Oxford Instruments), operated at 20 kV accelerating voltage with 1.1 nm lateral resolution, 20 nA current. BSE images of the nanostructures were obtained at 20 kV acceleration voltage. A Focus Ion Beam (FIB, Ga ions, acceleration voltage 30 kV) was used to polish the surface and to obtain high resolution secondary electron images (5 kV) of the nanoparticles when they were too small to be observed directly on the mechanically polished cross section.

The chemical composition of the glasses was measured using an Electron Microprobe JEOL JXA-8230 from Scientific and Technological Centers from University of Barcelona with five Wavelength-Dispersive X-Ray Spectroscopy (WDS) spectrometers, with probe current of 15 nA. Calibration was performed using mineral and glass standards, the oxygen content was calculated by stoichiometry. The totals varied between 98.4% and 101.2%. Other elements present below the detection limit of the microprobe (below 0.01%) were determined in some of the red glasses by Laser-Ablation ICP Mass spectrometry (LA-ICP-MS) (details on the analytical methods are found in Gratuze [24]).

The nature of the particles present in the red glasses was determined by micro-X-Ray Diffraction (micro-XRD). The micro-XRD patterns were obtained from thin cross sections (about 200 μm) cut from small fragments of the samples included in epoxy resin using a low speed diamond saw. Synchrotron micro-XRD patterns were collected in the Materials Science and Powder Diffraction beamline (MSPD BL04) [25], at the ALBA Synchrotron Light (Cerdanyola, Spain) in transmission geometry, using 0.4246 Å wavelength (29.2 keV), a 20 × 20 μm^2 spot size, 30s acquisition time and a CCD camera, SX165 (Rayonix, L.L.C., Evanston, IL) detector. The 2D images have been integrated using the d2Dplot program [26]. The XRD data has been identified using the Powder Diffraction File Database (PDF) from the International Centre for Diffraction Data (ICS) [27].

Ultraviolet–Visible (UV–Vis) diffuse absorption measurements were obtained in transmission mode using a double beam spectrophotometer (Shimadzu 2700) recorded between 200 nm and 800 nm, and NIR transmittance measurements using a double beam spectrophotometer (Shimadzu 3600) recorded between 800 nm and 3000 nm.

Fe, Cu and S K-edge micro-XAS data were acquired at the ID21 beamline, ESRF [28]. X-rays were produced with an undulator, and their energy was set using a Si(111) double crystal monochromator. For the analysis of the glass samples, the beam was focused to 0.3 × 0.9 μm^2 (v. × h.) using a Kirkpatrick Baez mirror system. Samples were mounted vertically, under an angle of 62° with respect to the incident beam. The samples were place in vacuum and the XAS Fluorescence data was collected using a single energy-dispersive silicon drift detector (SGX, 80 mm^2). For the Fe K-edge, the energy was scanned from 7.10 to 7.35 keV and for the Cu K-edge from 8.95 to 9.50 keV, both with steps of 0.5 eV and for the S K-edge, from 2.45 to 2.53 keV with a step of 0.3 eV. To avoid beam damage, the acquisition time was set at 0.1 s, each spectrum was collected only once on each point, and several spectra from different points were then averaged (at least even in the small copper sulphide particles), to reduce the cumulated dose, the XRF detector was placed as closed as possible to the sample and the flux was reduced using titanium and aluminium foils of various thicknesses and the scans were collected in "continuous" mode. The spectra are deadtime corrected and corrected by the beam intensity, measured continuously with a photodiode upstream the sample. The monochromator was calibrated using the first inflection point of copper and iron metallic foils (maximum of the first derivative at 7112 eV for Fe foil, 8979 eV for Cu foil) and the first feature of sodium thiosulphate ($Na_2S_2O_3{\cdot}5H_2O$) (2472 eV) using Athena software [29]. Spectra of some reference powders (Fe_2O_3, Fe_3O_4, Cu_2S, CuO and Cu_2O) spread on a piece of tape and covered with an ultralene foil were also acquired with an unfocussed beam (0.3 × 0.3 mm^2) in transmission mode.

XRF maps were first acquired at 9.5 keV, over 2D regions in order to locate the elements (notably Cu, Fe and S) and identify regions of interest. XRF batch fitting was done using Python scripts and the PyMca software [30]. From these maps, points of interest were selected on which XANES spectra were acquired, in XRF mode, at the Cu, Fe and S K-edge.

The copper speciation was obtained from the analyses of the Cu K-edge XAS spectra. As the glasses are essentially rich in oxygen (more than 80% of the atoms are oxygen), oxygen is the most probable nearest neighbour. Copper in magmas and in silicate glasses has been found to form complexes similarly to copper in aqueous solutions [31], with a higher intensity and slightly shifted relative to those of crystalline copper species. Cu K-edge XANES spectra for copper aqueous solutions appeared as copper-oxygen complexes in a distorted octahedral symmetry. Cu(I)-oxygen complexes have a very characteristic spectrum that displays a strong, rising resonance peak at ≈ 8983–8984 eV while Cu (II)-complexes have no pre-edge peak but the absorption maximum near 9000 eV [32,33]. Similarly, copper is present as a Cu(I)-oxide complex in sulphur-free and Low-S basaltic glasses obtained under reducing conditions [31]. Copper is considered a strongly chalcophile element and, consequently, it can also form complexes with S, Cu (I)-sulphide, the Cu K-edge spectral features of High-S basaltic glasses is similar to those of CuS (covellite) but smoother as corresponds to an amorphous structure [31]. In fact, various studies have shown that Cu^{2+} ions are not present in CuS, but that it has a pyrite-type structure where Cu^{1+} and S^{1-} undergo pairing [34]. Consequently, in our S-bearing glasses we may expect the presence of Cu(I)-oxide and Cu(I)-sulphide complexes besides the presence of crystalline metallic copper and copper sulphide particles. Fig. 2A shows the Cu K-edge XANES spectra corresponding to the different model compounds used in this study. Thanks to the micrometric beam size, the copper sulphide microparticles, and selected areas of the red glass near and far away from the particles were analysed. The red glass spectra fitting was carried out with Artemis software [29] as a linear combination of model compounds, Cu(I)-oxide [31], Cu(I)-sulphide and metallic Cu, each weighted by the compound fraction. The three-component fitting was done in the normalized μ(E) space over an energy range of 8960–9060eV. The calculated R factors (Table 3) are a measure of residuals between the fitted and measured spectra, lower R-factors correspond to a better fit [29]. The EXAFS region was also fitted giving similar results (about 5% of difference among them and 15% in the worst case).

Sulphur speciation was obtained from the analysis of the S K-edge spectra. S K-edge XANES allows non-destructive investigation of the coordination chemistry and oxidation state of sulphur species ranging from sulphide, S^{2-} to sulphate, S^{6+}. Sulphur species have a characteristic spectral feature representing the s→p and d-hybridization photoelectron transitions. On the contrary, the information that EXAFS can provide is limited because the oscillatory structure decays rapidly to a line past the edge [35]. S^{2-} or S^{6+} are generally agreed to dominate in silicate glasses rarely showing intermediate oxidation states [36,37] as the presence of sulphites is commonly attributed to beam damage. Fig. 2B shows the S K-edge XANES, corresponding to oxidised (dominant S^{6+}) and reduced (dominant S^{2-}) silicate glass [37]. Oxidised glasses show a sharp K-edge feature with respect to the sodium thiosulphate at about 2483.0 eV corresponding to S^{6+} while reduced glasses have a broad band at 2476.9 eV corresponding to S^{2-}. In our glasses sulphur was present dissolved both in the transparent base and in the red glass where it was also present forming copper sulphide particles.

With regard to iron, the Fe K-edge shifts to higher energies increasing the oxidation state of the iron specie. The energy shift may be estimated using the Integral Method [38], which determines the energy for which the same total absorption is obtained. The energy shift for the red and transparent glasses has been determined. The exact translation of this energy shift to the oxidation state of iron depends on the composition of the glasses. Nevertheless, a comparison among the glasses can be obtained.

The pre-edge feature of the Fe K-edge absorption is also particularly sensitive to the valence state and local geometry. The pre-peak related to

Fe^{3+} appears at about 7114.4 eV to Fe^{2+} at about 7112.7 eV (taking the first inflection of the metallic iron edge at 7112 eV). A centroid (CE) is calculated as the weighted position of the pre-peak region [38–40]. Therefore, the CE shifts to higher energy as the ratio of ferric to ferrous iron increases. The pre-edge region of the normalized X-ray absorption near-edge structure (XANES) spectra was analysed developing a python code [41] based on procedures described in literature. Considering the number of variables involved, imposing some restriction to the number of experimental parameters is advisable. For this reason, the Full Width at Half Maximum (FWHM) and Gaussian fraction were constrained to be shared by all peaks. Moreover, the Gaussian contribution dominates the peak profile of the pre-edge spectrum (XG >0.9) measured in standard resolution [40], and the FWHM of the standards was ≈2 eV. To avoid unrealistic fitting, we decided to fix the gaussian contribution to 1 and the FWHM to 2.1 eV. The centroid of the pre-peak has also been determined for the red and transparent glasses. The results are consistent with the data obtained with the Integral method.

3. Results

All the glasses show a characteristic sandwich-like structure (Fig. 1C, Fig. 3B), a red glass layer of about 100–300 μm thickness is applied over a transparent base glass of about 1–3 mm thickness and covered by a transparent glass of about 50–300 μm thickness. The cover layer is often highly corroded, with crystalline precipitates formed on many areas of the surface (Fig. 1B) making the glasses opaquer, and sometimes it is even missing.

Table 2 and Fig. 3C, show the chemical composition of the base, red and cover glasses. The composition of the three glasses is basically the same with the exception of copper; this indicates that copper was added to a transparent glass of similar composition to obtain the red glass. Between the 13th and the beginning of the 16th century the glasses are of the potash-lime type with increasing K_2O and CaO content in the 14th and 15th centuries (Fig. 3C). In the 16th century a sudden change in the glass composition happens in the form of an increase in the SiO_2, CaO and Al_2O_3 and decrease in the K_2O, P_2O_5 and MgO content (Fig. 3C). The amount of iron and manganese is low (below 0.9%FeO and below 1.1% MnO) in all the glasses. Tin is present in amounts below the detection limit of the microprobe, it has been determined by Laser-Ablation ICP Mass spectrometry (LA-ICP-MS) (details on the analytical methods are found in Gratuze [24]). Some of the samples (CB1, CB2, CB3, CB4, PS15 and Valls) tin contents vary between 2 and 50 ppm. Similarly, As varies between 10 and 50 ppm, Zn and Rb between 150 and 250 ppm, Zr between 100 and 150 ppm and Sr between 500 and 700 ppm. A few ppm of Ni, Co, Ag, Sn, Sb, Pb, As and Bi are also present. Potash-lime glasses were produced mixing sand which usually contains some clay and feldspars with forest wood ashes which are potash and lime rich but also contain small amounts of sulphur, phosphorous, chlorine, magnesium and manganese. Consequently, Ni, Co, Zn, Ag, Sn, Sb, Pb, As and Bi may be related to the source of copper while Zr, Sr and Rb to the sand.

A Cu/S atomic ratio ≈ 2 is determined for the Medieval glasses (2.5, 2.3, 2,6, 1.8, 2.3 and 1.9 ± 0.2 for SC13, CB3, CB4, CB5, CB1 and CB2 respectively see Table 2) and in some few copper sulphide particles are identified (Fig. 4A). On the contrary, the Renaissance glasses (PS15, SC14 and Valls) have a similar amount of copper but lower sulphur (for PS15 and Valls below detection limits of the Microprobe) and profuse copper sulphide particles (typical volume fraction of about 0.6%) are identified (Fig. 5A). We have to mention, that the analyses of the red glasses were performed in areas free of copper sulphide particles, thanks to the small beam size of the Microprobe ~ 1 μm^2 and large size of the copper sulphide particles (between 0.5 μm and 7 μm).

SEM images (Fig. 4B and D) of the Medieval red glass layers show the presence of metallic copper nanoparticles (typical sizes varying between 20 nm and 50 nm); SC13 shows also the presence of a few micron sized copper sulphide particles (Fig. 4A and C). In the Renaissance (PS15, SC14 and Valls) both micron sized copper sulphide particles (between 0.5 μm and 7 μm) (Fig. 5A, C and D), and metallic copper nanoparticles (typical sizes varying between 20 nm and 50 nm) (Fig. 5B and E), are found. The micro-XRD patterns taken from the Medieval red glass layers show the presence of metallic copper nanoparticles (ICCD file 01-85-1326) and in the Renaissance glasses (PS15, SC14 and Valls) also of tetragonal Cu_2S (chalcocite) (ICDD file 01-72-1071) particles (Figs. 4E and 5F).

The presence of copper sulphide precipitates is not unexpected in silicate melts. Copper is a high chalcophillic element and sulphur has very low solubility in a silicate melt. Consequently, a sulphide-silicate melt partition happens at high temperature in the melt with the precipitation of solid copper sulphide blebs (spherical inclusions) after cooling. In particular, the temperature at which copper sulphide separates from a basaltic melt depends also on the pressure; at low pressure,

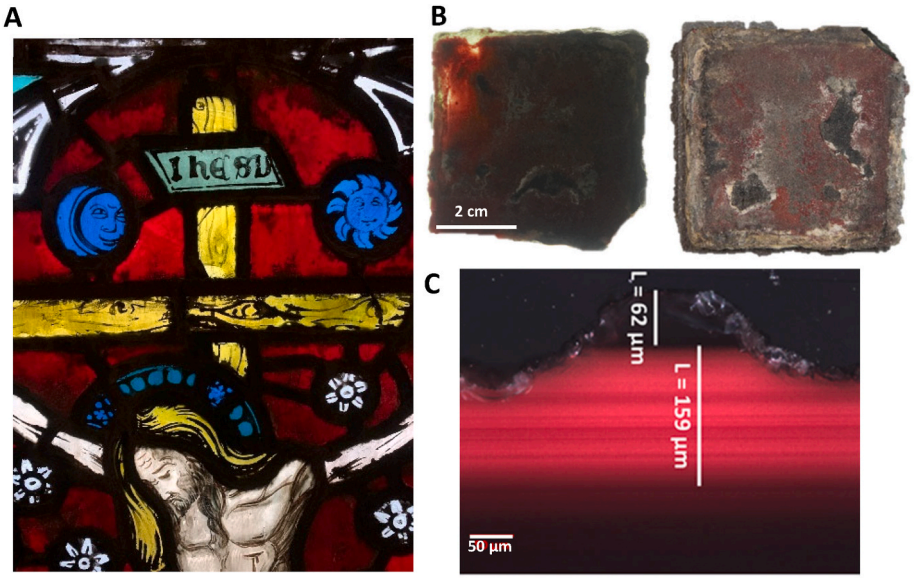

Fig. 1. (A) Scene from Santa Eulalia window, cathedral of Barcelona, c. 1330. (B) On the left, transmission and on the right, reflection image of the fragment from which the CB1 sample was cut and (C) dark field optical image of a cross section of CB1 from Sant Andreu & Sant Llorenç window, cathedral of Barcelona c. 1398–1408 by Nicoli de Maraye.

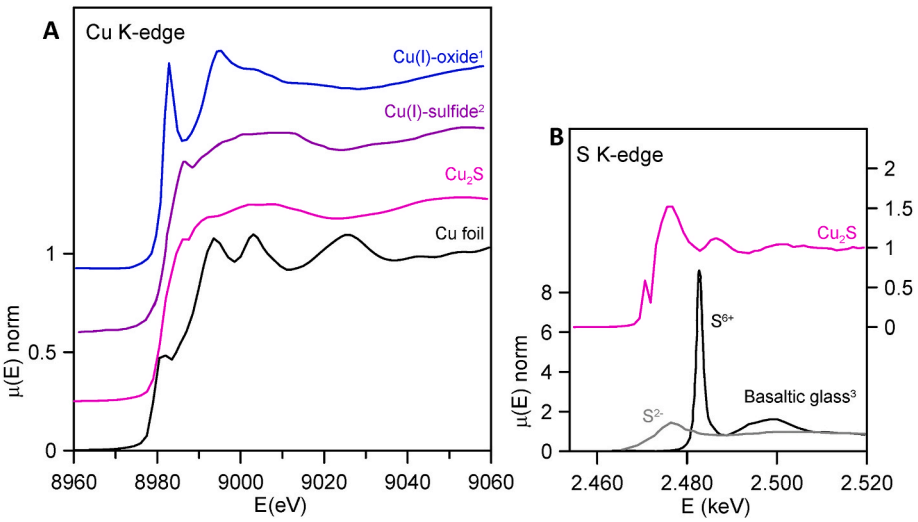

Fig. 2. (A) Cu K-edge XANES of the model compounds, [1]Cu(I)-oxide, Low-S basaltic glass spectrum and [2]Cu(I)-sulfide, High-S basaltic glass spectrum after Lanzirotti [31], Cu foil and Cu_2S (chalcocite) (B) S K-edge XANES, of the model compounds,[3]completely oxidised (black) and reduced (grey) basaltic glass after Jugo [37] and Cu_2S, chalcocite, (magenta) used to fit the red glasses. (For interpretation of the references to colour in this figure legend, the reader is referred to the Web version of this article.)

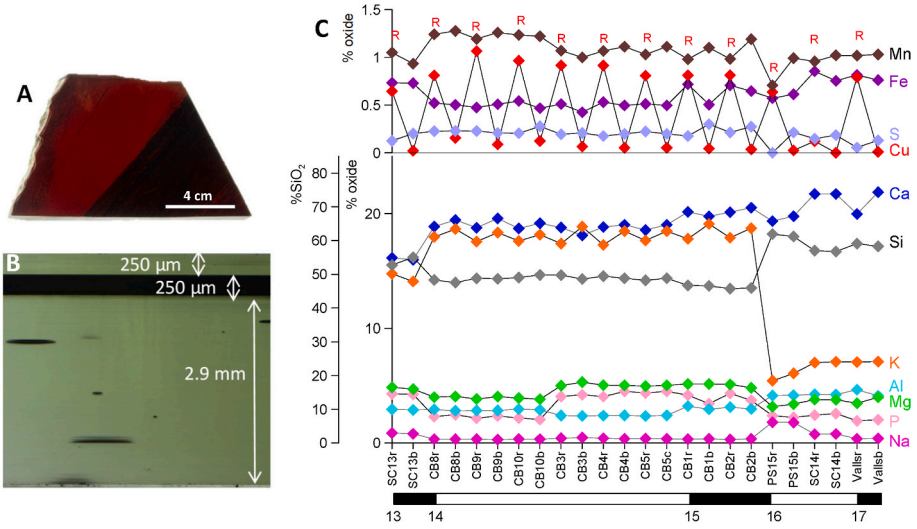

Fig. 3. (A) Glass fragment from cathedral of Segovia by Pierres d'Hollande & Pierres de Chiverri, 1544–1548 from which the sample PS15 was cut, (B) Optical transmission image of the polished cross section of PS15. (C) Chemical composition of all the red (r) and base (b) glasses analysed by Microprobe showing changes in the composition of glasses over time. (For interpretation of the references to colour in this figure legend, the reader is referred to the Web version of this article.)

the temperature may be extrapolated [42] between 1050°C and 1100 °C. The experiments performed [42,43] provided also evidence for oxide or oxy-sulphide complexing of Cu in the silicate melts, showing a decrease in the solubility of copper increasing the sulphur content of the melt (between some tens of ppm up to about 10^3 ppm). It should be noted that the composition of our glasses differs from basaltic glasses (it is richer in potassium and poorer in iron) and, consequently, the range of temperatures for which the silicate/sulphide partition happens does not necessarily coincide.

Among the impurities present in the glass which may produce sulphide precipitates Ni, Ag, Bi are the most probable and Co, Pb, Sn and Sb less probable [39]. In our case, from a few to some tens of ppm of Ni, Co, Ag, Sn, Sb, Pb and Bi are determined in the red glasses. In fact, in our glasses silver sulphide precipitates are also found (Fig. 4C). Although no other elements are found in the particles studied, they could also be present in the sulphide precipitates.

In order to understand the role of sulphur in the development of the red colour of the glasses Cu K-edge and S K-edge (only for SC13) micro-XANES spectra were obtained in different areas of the glasses and particles (Fig. 6).

Cu K-edge spectra were obtained from the red glass far from the copper sulphide particles, in the copper sulphide particles and in sulphur-poor areas of the copper sulphide particles (Fig. 6A). The data show that the red glass contains a large number of small metallic copper particles, and a few larger ones, of a composition consistent with Cu_2S; the spectra of the sulphur-poor areas in the particles show also mainly a copper sulphide shape but with some contribution of metallic copper. The red glass spectra can be fitted by a linear combination of metallic copper, copper(I)-oxide and copper(I)-sulphide complexes model compounds [31] following the procedure indicated in the *Materials and Methods* section. The results are shown in Fig. 7 and Table 3.

The data show that metallic copper and Cu(I)-oxide are present in all the red glasses analysed while Cu(I)-sulphide is also present in the Renaissance glasses (PS15 and Valls). S K-edge spectra were also obtained from different areas of SC13; the red and transparent glasses, the copper sulphide particles and around the copper sulphide particles (Fig. 6B). The data show that the sulphide particles spectra are consistent with Cu_2S. S^{6+} is determined in the transparent glass and in the red glass far away from the copper sulphide particles, while a mixture of S^{2-} and S^{6+} is found in the area around the copper sulphide particles. This result is in good agreement with the literature [36,37], S^{2-} and S^{6+} coexist in silicate melts while S^{4+} is absent or insignificant. The result is also

Table 2
Major and minor elements composition of the glasses. Microprobe analysis. bd: below detection limit. *cover glass was missing.

Sample	colour	SiO_2	Al_2O_3	TiO_2	CaO	Na_2O	MgO	BaO	MnO	FeO	CuO	K_2O	Cl	SO_3	P_2O_5	Tot	at%Fe	at%Cu	at%S
SC13	cover	54.3	2.86	0.16	16.0	0.83	4.76	0.31	0.98	0.68	bd	14.1	bd	0.20	4.21	99.4	0.21	0.00	0.11
	red	52.7	2.94	0.19	16.1	0.87	4.87	0.34	1.05	0.73	0.65	14.8	bd	0.13	4.30	99.7	0.23	0.17	0.07
	base	55.0	2.88	0.22	16.0	0.81	4.70	0.28	0.94	0.73	bd	14.1	bd	0.20	4.25	100.1	0.22	0.01	0.11
CB8*	red	48.3	2.93	0.23	18.9	0.33	4.01	0.90	1.24	0.52	0.81	18.0	0.12	0.23	2.30	98.8	0.17	0.23	0.13
	base	47.6	2.83	0.20	19.4	0.34	4.07	0.83	1.28	0.50	0.16	18.7	0.14	0.23	2.47	98.8	0.16	0.04	0.13
CB9	cover	48.7	2.84	0.18	19.6	0.30	4.05	0.91	1.26	0.51	0.09	18.3	0.13	0.21	2.36	99.4	0.15	0.02	0.16
	red	48.8	2.84	0.20	18.8	0.33	3.85	0.87	1.19	0.48	1.07	17.6	0.08	0.23	2.17	98.5	0.16	0.30	0.13
	base	48.6	2.83	0.17	19.6	0.32	4.02	0.84	1.21	0.46	0.07	18.5	0.11	0.29	2.18	99.2	0.16	0.02	0.12
CB10	cover	49.0	2.89	0.20	19.1	0.29	3.87	0.76	1.31	0.54	0.09	18.0	0.10	0.24	1.99	98.4	0.18	0.03	0.14
	red	49.0	2.96	0.20	18.7	0.33	3.92	0.94	1.23	0.54	0.97	17.6	0.04	0.21	2.18	98.8	0.18	0.27	0.12
	base	49.8	2.90	0.20	19.2	0.34	3.83	0.72	1.22	0.47	0.12	18.2	0.13	0.28	2.06	99.5	0.15	0.03	0.16
CB3	cover	49.0	2.37	0.11	19.2	0.40	5.04	0.36	1.06	0.49	bd	18.0	0.16	0.23	4.60	101.0	0.15	0.01	0.13
	red	49.7	2.40	0.12	18.8	0.42	5.01	0.37	1.07	0.51	0.92	17.4	0.15	0.19	4.06	101.1	0.16	0.25	0.11
	base	48.6	2.37	0.09	18.1	0.48	5.32	0.49	1.00	0.43	bd	18.9	bd	0.21	4.21	100.2	0.13	0.02	0.12
CB4	cover	49.0	2.40	0.14	19.0	0.38	5.03	0.39	1.09	0.50	bd	18.3	0.15	0.27	4.33	101.0	0.16	0.02	0.15
	red	49.4	2.39	0.12	18.8	0.42	5.05	0.39	1.07	0.53	0.91	17.3	0.14	0.18	4.05	100.8	0.17	0.25	0.10
	base	48.8	2.41	0.11	19.0	0.37	5.03	0.40	1.11	0.50	bd	18.5	0.16	0.20	4.51	101.1	0.16	0.01	0.11
CB5*	red	48.2	2.37	0.11	18.6	0.38	4.97	0.37	1.03	0.51	0.81	17.7	0.15	0.22	4.37	99.8	0.13	0.00	0.13
	base	47.4	2.32	0.16	18.4	0.38	5.26	0.50	0.99	0.40	bd	18.7	bd	0.22	4.20	98.9	0.16	0.23	0.12
CB1	cover	46.9	3.08	0.20	20.5	0.33	4.71	0.36	1.19	0.64	0.25	18.3	bd	0.28	3.50	100.2	0.21	0.07	0.16
	red	46.7	3.21	0.16	20.1	0.33	5.15	0.33	0.98	0.72	0.81	17.8	bd	0.18	4.18	100.7	0.23	0.23	0.10
	base	46.5	2.95	0.27	19.8	0.36	5.15	0.35	1.10	0.51	bd	19.1	bd	0.30	3.44	99.8	0.16	0.01	0.17
CB2	cover	45.9	3.01	0.21	20.5	0.33	4.94	0.37	1.17	0.65	0.30	18.3	bd	0.26	3.43	99.4	0.21	0.09	0.15
	red	45.7	3.13	0.14	20.1	0.31	5.12	0.36	0.98	0.71	0.81	17.9	bd	0.21	4.33	99.8	0.23	0.23	0.12
	base	45.9	2.98	0.12	20.5	0.36	4.82	0.42	1.19	0.65	bd	18.7	bd	0.27	3.73	99.6	0.21	0.01	0.16
PS15	cover	61.2	4.16	0.21	19.6	1.92	3.33	0.25	0.83	0.60	0.16	5.50	0.52	0.18	2.33	100.8	0.17	0.04	0.09
	red	61.9	4.15	0.22	19.3	1.81	3.17	0.20	0.71	0.57	0.64	5.44	0.45	bd	2.39	101.0	0.16	0.16	0.00
	base	61.2	4.16	0.21	19.8	1.79	3.39	0.27	0.99	0.61	bd	6.08	0.53	0.21	2.24	101.2	0.18	0.01	0.11
SC14	cover	57.0	4.23	0.27	22.0	0.80	3.80	0.41	0.97	0.72	bd	7.09	bd	0.18	2.65	100.1	0.21	0.00	0.09
	red	57.0	4.25	0.25	21.7	0.77	3.80	0.43	0.96	0.86	0.12	7.02	bd	0.15	2.43	99.7	0.25	0.03	0.08
	base	56.7	4.23	0.31	21.7	0.79	3.78	0.30	1.02	0.76	bd	7.09	bd	0.19	2.57	99.4	0.22	0.00	0.10
Valls	cover	58.9	4.01	0.23	21.2	0.39	3.70	0.41	0.94	0.84	bd	6.78	bd	0.27	2.03	99.7	0.25	0.00	0.14
	red	59.1	4.66	0.24	20.0	0.38	3.47	0.41	1.02	0.82	0.79	7.07	bd	bd	1.94	99.9	0.24	0.21	0.03
	base	58.2	4.12	0.20	21.9	0.40	3.99	0.38	1.03	0.76	bd	7.11	bd	0.13	2.03	100.3	0.22	0.00	0.07

Table 3
Copper XANES speciation calculated using a linear combination of Cu(I)-oxide (Low-S basaltic glass) and Cu(I)-sulphide (High-S basaltic glass) after Lanzirotti [31] and metallic Cu.

Red glass	Cu(I)-sulphide (%)	Cu(I)-oxide (%)	Cu^{o} (%)	R factor (%)
SC13	–	37(1)	63(1)	0.05
CB5	–	58(3)	40(3)	0.50
CB2	–	52(2)	46(2)	0.30
PS15	16(2)	54(1)	29(1)	0.20
Valls	26(3)	38(2)	35(2)	0.10

consistent with the fact that S^{2-} is pretty insoluble compared to S^{6+} in a silicate melt and, consequently, a higher concentration of S^{6+} can be present in the silicate melt without saturation or precipitation of sulphate compounds, while relatively low S contents (as S^{2-}) is required to reach sulphide saturation [37].

Moreover, the transition from S^{2-} to S^{6+} in silicate melts occurs over a very narrow interval of oxygen fugacity contrarily to the transition from Fe^{2+} to Fe^{3+} which expands over 16 orders of magnitude [44]. Consequently, a slight increase in the oxygen fugacity results in a fast transformation of S^{2-} into S^{6+}. Finally, although sulphur occurs as sulphide (S^{2-}), sulphate (S^{6+}) or a combination of both in the silicate melts, it can also be released as SO_2 (S^{4+}), secondly as H_2S and in minor amounts as S_2 and COS [37]. Therefore, the release of S to the atmosphere during the glass firing cannot be withdrawn.

To investigate the role of iron in the process, Fe K-edge spectra were also obtained from the red and transparent glasses from the Medieval (SC13, CB5) and Renaissance (PS15 and Valls) periods. Fig. 8 shows also a different behaviour for the Medieval and Renaissance glasses. While in the Medieval glasses SC13 and CB5, the red glass is more oxidised than the transparent glass, in the Renaissance glasses PS15 and Valls, the transparent glass is more oxidised than the red glass. The data indicates a more oxidising atmosphere for the red Medieval glasses and a more reducing atmosphere for the red Renaissance glasses.

Although the precipitation of copper sulphide is expected in silicate melts containing sulphur, the precipitation of tetragonal chalcocite was not expected. Chalcocite at room temperature is monoclinic and inverts to hexagonal at 103°C; at 435°C the cubic high polymorph forms continuous solid solution with cubic $Cu_{9+x}S_5$ [45]. At low-temperature, a high-pressure polymorph stable only above ~0.8 kbars has tetragonal symmetry [46]. Therefore, at room temperature and pressure, monoclinic chalcocite should be formed. However, some studies have demonstrated the stabilisation of tetragonal chalcocite in presence of Fe^{3+} [47]. The stabilisation of tetragonal chalcocite seems therefore related to the presence of iron in the melt.

The cubic crystallographic structure of tetragonal chalcocite is particularly interesting as while S atoms maintain a rigid sublattice, interstitial Cu atoms are distributed throughout many possible positions (up to 25). This high degree of structural disorder is also related to a high mobility of copper ions with temperature, resulting in a 'liquid-like' behaviour of copper ions around a crystalline sublattice [48,49].

Finally, UV–Vis–NIR analysis of the red glasses was also performed to assess the nature of the particles present (Fig. 9A), and colour coordinates (a^* and b^*) of the red glasses, Fig. 9B. Small metallic copper nanoparticles have a strong Surface Plasmon Resonance absorption band (SPR) at about 560 nm, responsible for the red colour of the glasses. On the contrary, copper sulphide particles absorb light in the Near-Infrared (NIR) region (above 800 nm) and, therefore, they do not contribute to the red colour of the glasses. The hue calculated by the slope of the line, in the colour wheel, Fig. 9B, is similar for all the red glasses (fitted value $h^* = 22.0(9)^{o}$, $r^2 = 0.998$). This indicates that copper nanoparticles present have a similar size for all the glasses

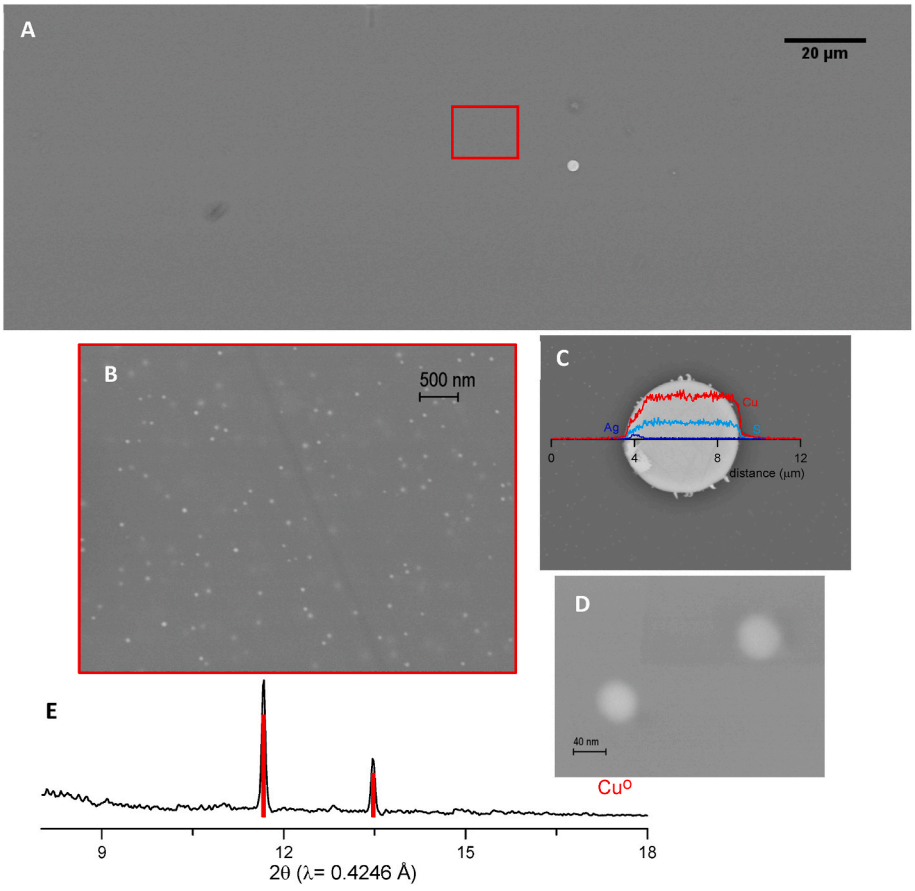

Fig. 4. (A) SEM-BSD image of a Medieval red glass SC13 (1284–1320, Monastery of Santes Creus. Tarragona) showing the presence of a micrometric Cu_2S particle (B) Magnification of the red square area from (A) showing the presence of small metallic copper nanoparticles. (C) Magnification and S, Cu and Ag linescan corresponding to one of the Cu_2S particles showing the presence of Ag_2S precipitated at the edge and (D) magnification of the metallic copper nanoparticles. (E) Micro-XRD pattern taken from a cross section of the red glass showing the presence of metallic copper, ICCD file 01-85-1326. (For interpretation of the references to colour in this figure legend, the reader is referred to the Web version of this article.)

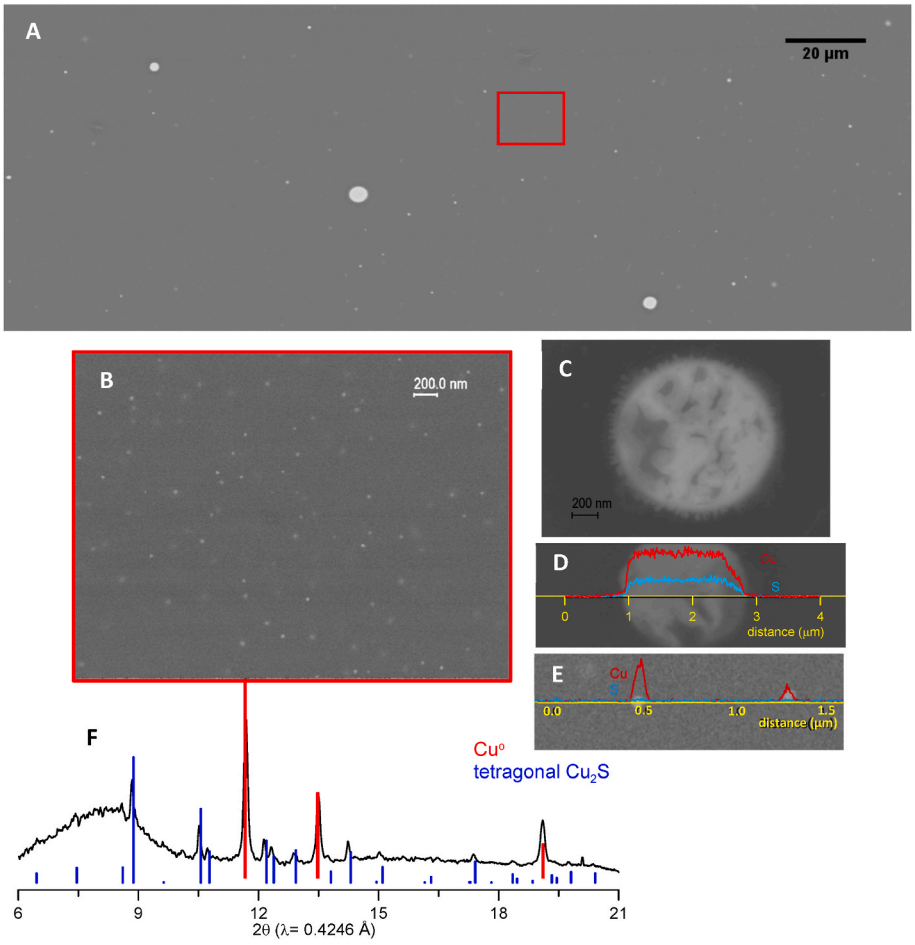

Fig. 5. (A) SEM-BSD image of a Renaissance red glass sample, Valls (Church of Sant Joan Baptiste de Valls, from the rose window by Giacomo Carnobali, c.1609) showing the presence of abundant micrometric Cu_2S particles (B) Magnification of the red square area from (A) showing the presence of small metallic copper nanoparticles. (C) Magnification and (D) Cu and S linescan corresponding to a large micrometric Cu_2S particle and (E) chemical linescan of the small nanometric metallic copper particles. (F) Micro-XRD pattern taken from a cross section of the red glass showing the presence of tetragonal Cu_2S, chalcocite, ICDD pattern 01-72-1071 and metallic copper, ICCD file 01-85-1326. (For interpretation of the references to colour in this figure legend, the reader is referred to the Web version of this article.)

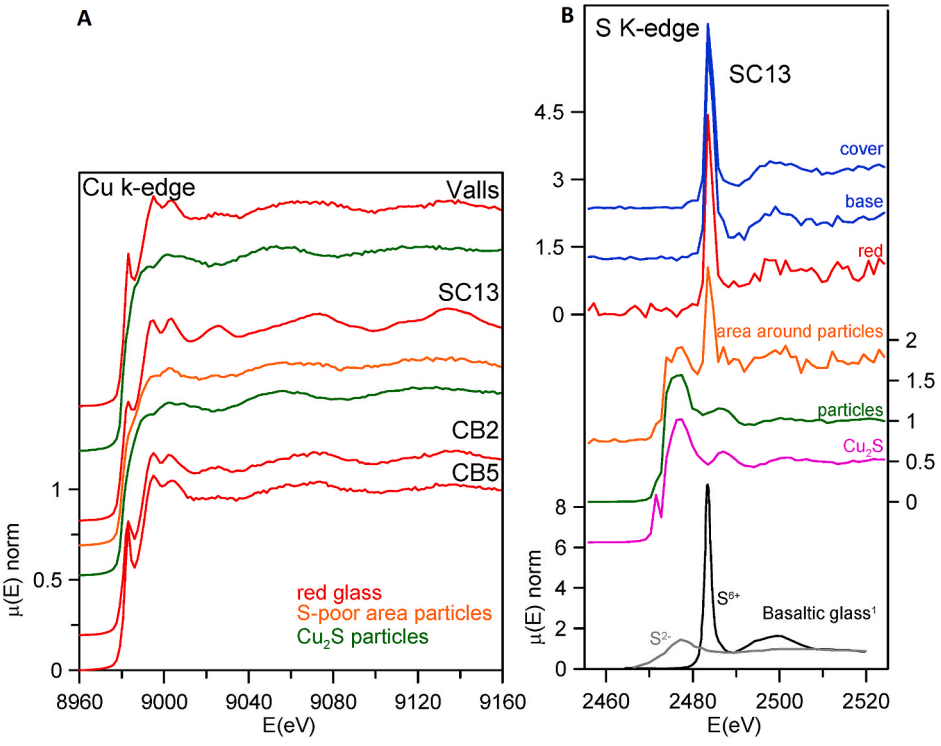

Fig. 6. (A) Copper K-edge XAFS of the red glass, copper sulphide particle and glass area around the particle of SC13 (1284–1320. Monastery of Santes Creus. Tarragona) and Valls (c.1609. Church of Sant Joan Baptiste de Valls) and of the red glasses from CB5 (1386. Cathedral. Barcelona) and CB2 (1398–1408. Cathedral. Barcelona) samples. (B) S K-edge XANES of SC13 transparent base and cover glasses and red glass, copper sulphide particle and glass area around the copper sulphide particle showing that sulphur in the glass areas is mainly present as S^{6+}. Reference spectra corresponding to Cu_2S (magenta) and a completely oxidised (black) (S^{6+}) and reduced (grey) (S^{2-}) basaltic glass after Jugo [37]. (For interpretation of the references to colour in this figure legend, the reader is referred to the Web version of this article.)

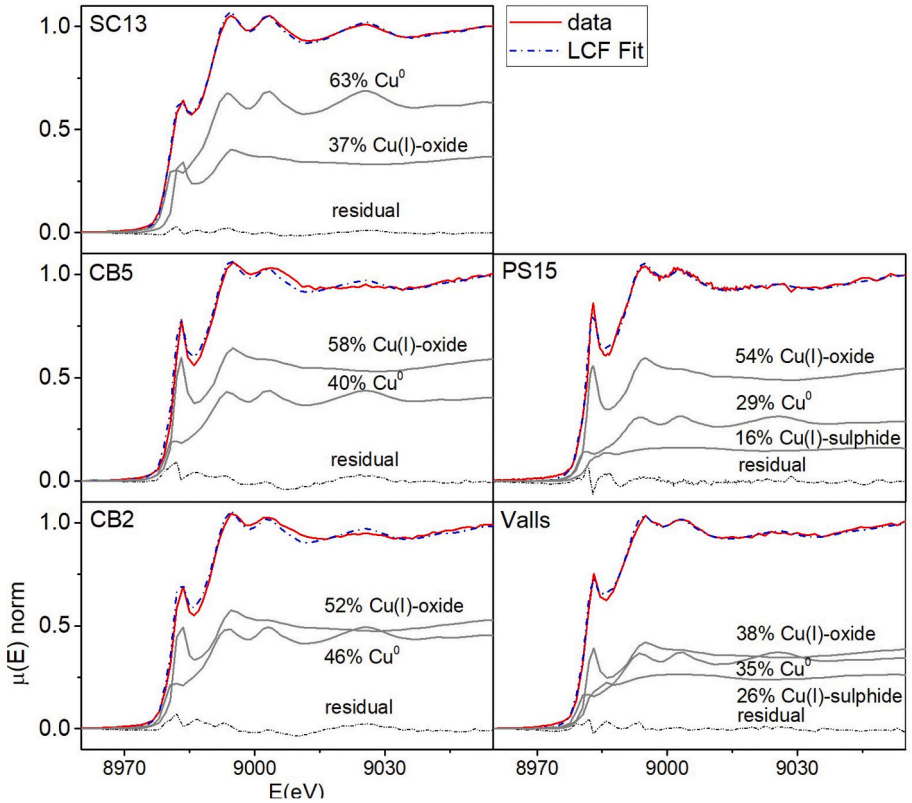

Fig. 7. Linear combination fitting of the Cu k-edge XANES spectra corresponding to the Medieval (SC13, CB5, CB2) and Renaissance (PS15 and Valls) red glasses using metallic copper (Cu^0), Cu(I)-oxygen and Cu(I)-sulphide complexes after Lanzirotti [31]. (For interpretation of the references to colour in this figure legend, the reader is referred to the Web version of this article.)

studied (below 50 nm). Lightness (L^*) and saturation (c^*) vary among the samples depending on the thickness and fraction of metallic copper nanoparticles of the red glass layer, but also on the thickness of the transparent base and cover glasses and the presence of alteration compounds at the surface which strongly reduce the light transmitted.

4. Discussion

The presence of small metallic copper nanoparticles absence of other copper precipitates such as cuprite is responsible for the ruby red colour of the glasses. Due to the limited solubility of metallic copper in a silicate melt, copper has to be previously oxidised. Consequently, in order to render the ruby red colour, reducing agents have to be incorporated in the melt to induce the precipitation of metallic copper.

Small amounts of sulphur were present (associated with the plant ashes) in the glasses from the Medieval and Renaissance period. Sulphur can be present in a silicate melt as S^{2-} or S^{6+} the first predominates when the melt is fired under reducing and the second when it is fired under oxidising conditions. Nevertheless, the solubility of sulphur in the melt is very low, in particular for S^{2-} and a sulphide-silicate melt partition happens, about ~1100°C extrapolated from the behaviour of basaltic glasses and also consistent with a recent replication of red glass [18]. As copper is a highly chalcophillic element, copper accumulates in the sulphide partition and during the cooling of the melt (Cu_2S) particles are formed. The presence of Fe^{3+} in the melt may be responsible for the stabilisation of tetragonal chalcocite the high-pressure tetragonal polymorph of chalcocite [47] rather than the low temperature/pressure form.

The Medieval glasses studied show that sulphur is present in the glass as S^{6+}, copper is present either as Cu^+ in the glass and forming metallic copper nanoparticles. Very few copper sulphide particles of tetragonal chalcocite (Cu_2S) are found. Sulphur is present as S^{2-} and S^{6+} in the glass around the particles and as S^{6+} in the glass. Therefore, we believe that during glass melting the equilibrium between ionic species causes sulphur to oxidise to S^{6+} while copper is reduced to the metallic state. The transition from Fe^{2+} to Fe^{3+} expands over a large oxygen fugacity range contrarily to the transition from S^{2-} to S^{6+}. Therefore, it is more likely that iron acted as an oxidation/reduction buffer, becoming more reduced or oxidised by the atmosphere rather than directly intervening in the reduction of copper to the metallic state and consequent precipitation of the copper nanoparticles.

In the Renaissance glasses, probably due to the use of a more reducing atmosphere and favoured by the different composition of the glasses, silica richer, iron appears more reduced, little sulphur is dissolved in the glass and a large number of copper sulphide particles also of tetragonal chalcocite (Cu_2S) occurs. In this case, metallic copper nanoparticles are also found in the glass but in a lower amount than in the Medieval glasses (about 30%–35% for the Renaissance glasses compared to 40–63% for the Medieval glasses) (Table 3). Iron is more reduced in the red glass than in the clear base glass which is also consistent with the use of more reducing conditions during the glass melting. And, in this case, iron cannot be responsible for the reduction of copper to the metallic state.

Then, to blow the glass, it is reheated in the air to the working temperature (~ 1050°C). At this temperature not only the glass but also the copper sulphide particles (melting point 1030°C) are liquid. Reheating of the glass is mentioned in the treatises as sometimes necessary for the glass to develop the red colour (*striking*). During this, S^{2-} present in the melt will be oxidised and copper reduced to the metallic state. The presence of both S^{2-} and S^{6+} in the glass around the particles and the peculiar hollow-like structure shown by the copper sulphide particles (Fig. 5), indicate that during the reheating of the glass some particles decompose. This would result in the precipitation of metallic copper nanoparticles. The high mobility of copper ions with

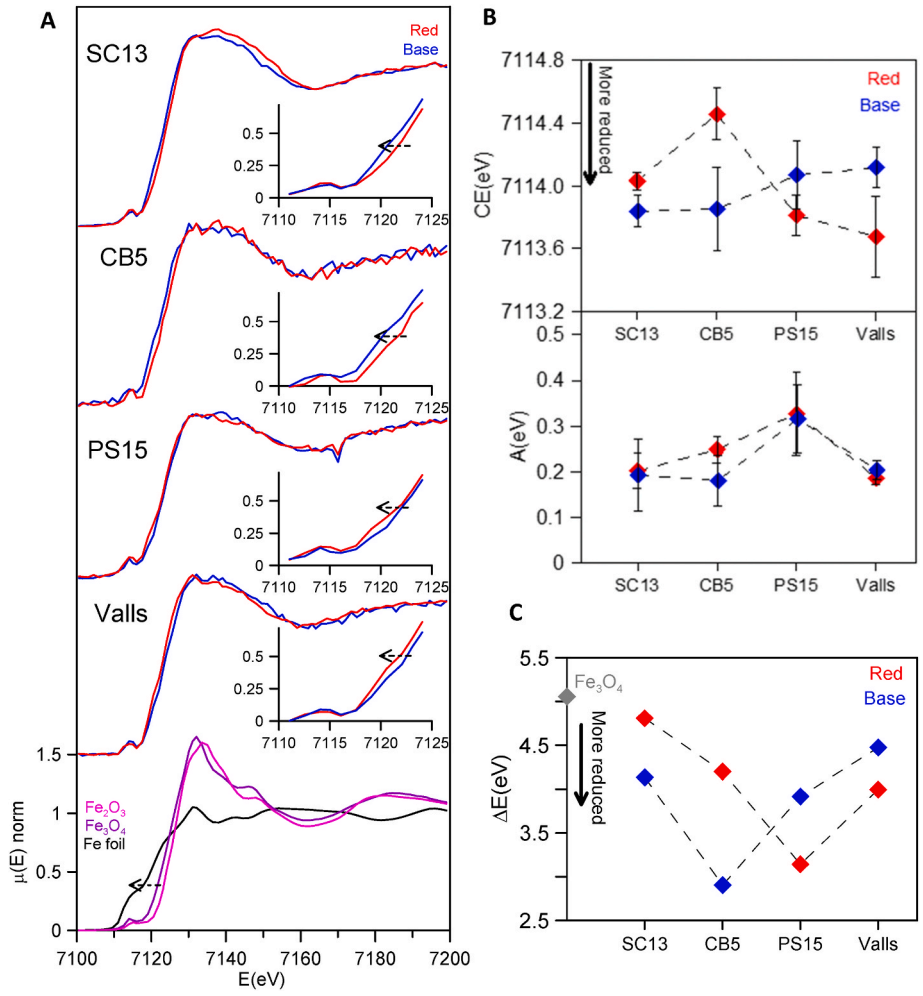

Fig. 8. (A) Fe K-edge spectra corresponding to the transparent and red glasses of the Medieval (SC13, CB5) and Renaissance (PS15 and Valls) and to the standards. (B) Centre shift (CE) and total Area (A) of the pre-peak [38,39] and (C) edge shift calculated using the Integral method. (For interpretation of the references to colour in this figure legend, the reader is referred to the Web version of this article.)

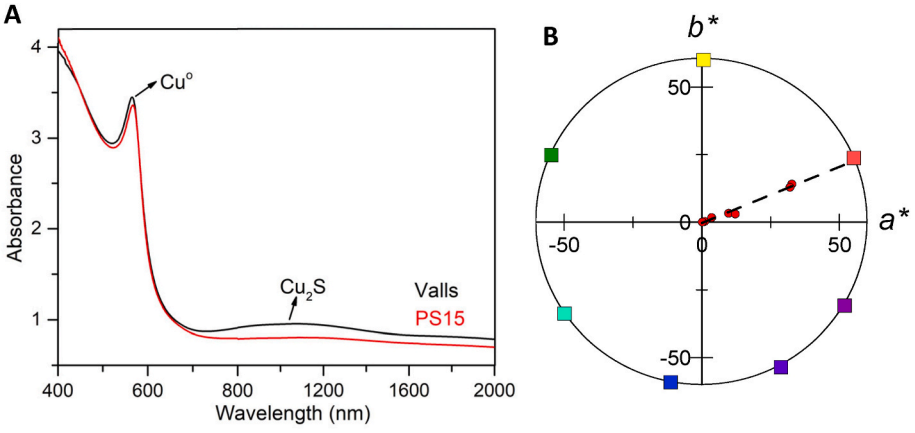

Fig. 9. (A) UV–Vis and NIR absorbance corresponding to Renaissance (PS15 and Valls) red glasses showing the characteristic Surface Plasmon Resonance peak corresponding to the metallic copper nanoparticles and a broad absorption peak in the NIR related to the Cu_2S precipitates. (B) CIE $L^*a^*b^*$ colour coordinates, a^* and b^* of the red glasses analysed (red dots) and fitted h^* (hue) (dotted line). (For interpretation of the references to colour in this figure legend, the reader is referred to the Web version of this article.)

temperature in tetragonal chalcocite [48,49] can favour this.

5. Conclusions

The ruby red colour of the glasses is obtained thanks to the presence of small metallic copper nanoparticles. Small amounts of sulphur were present in the Medieval and Renaissance red glasses. Sulphur has a low solubility in a silicate melt and is present as S^{2-} and/or S^{6+}. S^{6+} is more soluble than S^{2-}, consequently, a sulphide-silicate partition at a temperature above 1100°C is obtained; copper is a highly chalcophillic element and accumulates in the sulphide partition. The presence of iron in the melt may be responsible for the precipitation of tetragonal rather than monoclinic chalcocite (Cu_2S) particles. During the melting and/or reheating of the glass at high temperature under oxidising conditions,

sulphur is oxidised and copper reduced to the metallic state (*striking*). The differences found between Medieval and Renaissance red glasses may be related to the different composition, silica richer in the Renaissance glasses, or to more reducing conditions in the melting.

In summary, our data shows that sulphur was a key ingredient in the production of the red glasses of the period, in agreement with the main conclusions obtained from the replication of red glass following some historical recipes. On the contrary, iron does not seem to have a direct role in the reduction of copper and the precipitation of copper nanoparticles but rather an indirect role stabilizing tetragonal chalcocite and acting as an oxidation/reduction buffer.

Funding

This work received financial support from MINECO (Spain) (grant PID2019-105823RB-I00), the Generalitat de Catalunya (grant 2021 SGR 00343), ESRF (https://doi.org/10.15151/ESRF-ES-879445008) and ALBA synchrotron Facility number (2020094561).

Declaration of competing interest

The authors declare that they have no known competing financial interests or personal relationships that could have appeared to influence the work reported in this paper.

Acknowledgements

The XAS experiments were performed at ID21 Beamline at ESRF with the collaboration of ESRF Staff, through the proposal HG-172. Micro-XRD experiments were performed at BL04 (MSPD) Beamline at ALBA synchrotron Facility with the collaboration of Alba Staff. Vetraria Muñoz de Pablos S.L. and in particular Pablo and Alfonso are thanked for providing one of the glass pieces studied.

References

[1] C. Noirot, L. Cormier, N. Schibille, N. Menguy, N. Trcera, E. Fonda, Comparative investigation of red and orange roman tesserae: role of Cu and Pb in colour formation, Heritage 5 (3) (2022) 2628–2645, https://doi.org/10.3390/heritage5030137.

[2] W.A. Weyl, Coloured Glasses, Reprint by Society of Glass Technology, Sheffield, 1951, 1976.

[3] S. Ishida, M. Hayashi, N. Takeuchi, M. Wakamatsu, Role of Sn^{2+} in development of red colour during reheating of copper glass, J. Non-Cryst. Solids 95–96 (1987) 793–800, https://doi.org/10.1016/S0022-3093(87)80683-X.

[4] I.C. Freestone, London, in: M. Bimson, I.C. Freestone (Eds.), Composition and Microstructure of Early Opaque Red Glass in Early Vitreous Materials, British Museum Occasional Paper 56, 1987, pp. 173–191, 13: 9780861590568.

[5] I.C. Freestone, Theophilus and the composition of medieval glass, MRS Online Proc. Libr. 267 (1992) 739–745, https://doi.org/10.1557/PROC-267-739.

[6] I. Nakai, C. Numako, H. Hosono, K. Yamasaki, Origin of the red color of satsuma copper-ruby glass as determined by EXAFS and optical absorption spectroscopy, J. Am. Ceram. Soc. 82 (3) (1999) 689–695, https://doi.org/10.1111/j.1151-2916.1999.tb01818.x.

[7] F. Farges, M.-P. Etcheverry, A. Scheidegger, D. Grolimund, Speciation and weathering of copper in "copper red ruby" medieval flashed glasses from the Tours cathedral (XIII century), Appl. Geochem. 21 (2006) 1715–1731, https://doi.org/10.1016/j.apgeochem.2006.07.008.

[8] J.J. Kunicki-Goldfinger, I.C. Freestone, I. McDonald, J.A. Hobot, H. Gilderdale-Scott, T. Ayers, Technology, production and chronology of red window glass in the medieval period-rediscovery of a lost technology, J. Archaeol. Sci. 41 (2014) 89–105, https://doi.org/10.1016/j.jas.2013.07.029.

[9] T. Pradell, Lustre and nanostructures-ancient technologies revisited, in: P. Dillmann, L. Bellot-Gurlet, I. Nenner (Eds.), Nanoscience and Cultural Heritage, Atlantis Press, Paris, 2019, https://doi.org/10.2991/978-94-6239-198-7_1.

[10] G. Li, Y. Lei, The computational simulation of the reflection spectra of copper red glaze, AIP Adv. 12 (9) (2022), 095319, https://doi.org/10.1063/5.0095570.

[11] M.P. Alonso, F. Capel, F.J. Valle Fuentes, A. De Pablos, I. Ortega, B. Gómez, M. A. Respaldiza, Caracterización de un vidrio rojo medieval procedente de las vidrieras del Monasterio de las Huelgas de Burgos, Bol. Soc. Esp. Ceram. 8 (4) (2009) 179–186.

[12] T. Bring, B. Jonson, L. Kloo, J. Rosdahl, Colour development in copper ruby alkali silicate glasses. Part 1. The impact of tin oxide, time and temperature, Glass, Technol.: Eur. J. Glass Sci. Technolo. A. 48 (2) (2007) 101–108.

[13] T. Pradell, G. Molina, S. Murcia, R. Ibañez, C. Liu, J. Molera, A.J. Shortland, Materials, techniques, and conservation of historic stained glass "grisailles", Int. J. Appl. Glass Sci. 7 (1) (2016) 41–58, https://doi.org/10.1111/ijag.12125.

[14] P. Colomban, A. Tournié, P. Ricciardi, Raman spectroscopy of copper nanoparticle-containing glass matrices: ancient red stained-glass windows, J. Raman Spectrosc. 40 (2009) 1949–1955, 1949–195510.1002/jrs.2345.

[15] J.G. Hawthorne, C.S. Smith, Theophilus: on Divers Arts. The Foremost Medieval Treatise on Painting, Glassmaking and Metalwork, Dover Publications Inc., New York, 1979, 13:9780486237848.

[16] M. Cable, in: Michael Cable (Ed.), The World's Most Famous Book on Glassmaking: the Art of Glass by Antonio Neri, Christopher Merrett (Transl.), The Society of Glass Technology, Sheffield, 2001, 090068237X.

[17] J. Kunckel, Ars Vitraria Experimentalis, Oder Vollkommene Glasmacher-Kunst (Franckfurt und Leipzig, 1679), Deutches Textarchiv, http://www.deutschestextarchiv.de/kunckel_glasmacher_1679.

[18] M. Vilarigues, R. Ruivo, T. Hagendijk, M. Bandiera, M. Coutinho, L.C. Alves, S. Dupré, Red glass in Kunckel's Ars Vitraria Experimentalis: the importance of temperature, Int. J. Appl. Glass Sci. (2022) 1, https://doi.org/10.1111/ijag.16605. –15.

[19] D. Gimeno, M. Garcia-Valles, J.L. Fernandez-Turiel, F. Bazzocchi, M. Aulinas, M. Pugès, C. Tarozz, M.P. Riccardi, E. Basso, C. Fortina, M. Mendera, B. Messiga, From Siena to Barcelona: deciphering colour recipes of Na-rich Mediterranean stained glass windows at the XIII-XIV century transition, J. Cult. Herit. 9 (2008) e10–e15, https://doi.org/10.1016/j.culher.2008.08.001.

[20] M.C. Domínguez Rodés, S. Cañellas, Materials for stained glass windows in Catalonian documentation (14^{th} and 15^{th} centuries), J. Cult. Herit. 9 (2008) e85–e88, https://doi.org/10.1016/j.culher.2008.05.004.

[21] J. Ainaud i de Lasarte, J. Vila-Grau, M.J. Virgili, Els vitralls del monestir de Santes Creus i la Catedral de Tarragona, in: Corpus Vitrearum Medii Aevi. Catalunya, vol. 3, Institut d'Estudis Catalans, Barcelona, 1992, 84-7283-209-0.

[22] J. Ainaud i de Lasarte, A.M. Mundó, J. Vila-Grau, M.A. Escudero I Ribot, S. Cañellas, A. Vila i Delclòs, Els vitralls de la catedral de Barcelona i del monestir de Pedralbes, in: Corpus Vitrearum Medii Aevi. Catalunya, vol. 4, Institut d'Estudis Catalans, Barcelona, 1997, 84-7283-335-6.

[23] A. Velasco, S. Cañellas, El pas per Tàrrega del vitraller Jaume Carnoval (1608), URTX revista cultural de l'Urgell 31 (2017) 166–177. https://raco.cat/index.php/Urtx/article/view/326036.

[24] B. Gratuze, Glass characterization using laser ablation-inductively coupled plasma-mass spectrometry methods, in: L. Dussubieux, M. Golitko, B. Gratuze (Eds.), Recent Advances in Laser Ablation ICP-MS in Archaeology, Springer Verlag, Berlin Heidelberg, Natural Sciences in Archaeology, 2016, pp. 179–196, https://doi.org/10.1007/978-3-662-49894-1. Chap. 12.

[25] F. Fauth, I. Peral, C. Popescu, M. Knapp, The new material science powder diffraction beamline at ALBA synchrotron, Powder Diffr. 28 (S2) (2013), https://doi.org/10.1017/S0885715613000900. S360–S370.

[26] O. Vallcorba, J. Rius, d2Dplot: 2D X-ray diffraction data processing and analysis for through-the-substrate microdiffraction, J. Appl. Crystallogr. 52 (2019) 478–484, https://doi.org/10.1107/S160057671900219X.

[27] ICCDD, Web site of the international Centre for diffraction data. https://www.icdd.com/.

[28] M. Cotte, E. Pouyet, M. Salomé, C. Rivard, W. De Nolf, H. Castillo-Michel, T. Fabris, et al., The ID21 X-ray and infrared microscopy beamline at the ESRF: status and recent applications to artistic materials, J. Anal. At. Spectrom. 32 (2017) 477–493, https://doi.org/10.1039/C6JA00356G.

[29] B. Ravel, M. Newville, ATHENA, artemis, hephaestus: data analysis for X-ray absorption spectroscopy using IFEFFIT, J. Synchrotron Radiat. 12 (2005) 537–541, https://doi.org/10.1107/S0909049505012719.

[30] V.A. Sole, P. Papillon, M. Cotte, P. Walter, J. Susini, A multiplatform code for the analysis of energy-dispersive X-ray fluorescence spectra, J. Spectrochim. Acta B: At. Spectrosc. 62 (1) (2007) 63–68, https://doi.org/10.1016/j.sab.2006.12.002.

[31] A. Lanzirotti, L. Lee, E. Head, S.R. Sutton, M. Newville, M. McCanta, A.H. Lerner, P. J. Wallace, Direct measurements of copper speciation in basaltic glasses: understanding the relative roles of sulfur and oxygen in copper complexation in melts, Geochem. Cosmochim. Acta 267 (2019) 164–178, https://doi.org/10.1016/j.gca.2019.09.029.

[32] J.L. Fulton, M.M. Hoffmann, J.G. Darab, An X-ray absorption fine structure study of copper (I) chloride coordination structure in water up to 325°C, Chem. Phys. Lett. 330 (3–4) (2000) 300–308, https://doi.org/10.1016/S0009-2614(00)01110-6.

[33] J.L. Fulton, M.M. Hoffmann, J.G. Darab, B.J. Palmer, E.A. Stern, Copper (I) and copper (II) coordination structure under hydrothermal conditions at 325°C: an X-ray absorption fine structure and molecular dynamics study, J. Phys. Chem. A 104 (2000) 11651–11663, https://doi.org/10.1021/jp001949a.

[34] J. R Vegelius, K.O. Kvashnina, H. Hollmark, M. Klintenberg, Y.O. Kvashnin, I. L. Soroka, L. Werme, S.M. Butorin, X-ray spectroscopic study of Cu_2S, CuS, and copper films exposed to Na_2S solutions, J. Phys. Chem. C 116 (2012) 22293–22300, https://doi.org/10.1021/jp302390c.

[35] M.E. Fleet, X.Y. Liu, S.L. Harmer, P.L. King, Sulfur K- edge XANES spectroscopy: chemical state and content of sulfur in silicate glasses, Can. Mineral. 43 (2005) 1605–1618, https://doi.org/10.2113/gscanmin.43.5.1605.

[36] L. Backnaes, J. Stelling, H. Behrens, J. Goettlicher, S. Mangold, O. Verheijen, R.G. C. Beerkens, J. Deubener, Dissolution mechanisms of tetravalent sulphur in silicate melts: evidences from sulphur K edge XANES studies on glasses, J. Am. Ceram. Soc. 91 (3) (2008) 721–727, https://doi.org/10.1111/j.1551-2916.2007.02044.x.

[37] P.J. Jugo, M. Wilke, R.E. Botcharnikov, Sulfur K-edge XANES analysis of natural and synthetic basaltic glasses: implications for S speciation and S content as

function of oxygen fugacity, Geochem. Cosmochim. Acta 74 (20) (2010) 5926–5938, https://doi.org/10.1016/j.gca.2010.07.022.
[38] M. Wilke, F. Farges, P. Petit, G.E. Brown Jr., F. Martin, Oxidation state and coordination of Fe in minerals: an Fe K-XANES spectroscopic study, Am. Mineral. 86 (5) (2001) 714–730, https://doi.org/10.2138/am-2001-5-612.
[39] M. Wilke, G.M. Partzsch, R. Bernhardt, D. Lattard, Determination of the iron oxidation state in basaltic glasses using XANES at the K-edge, Chem. Geol. 220 (2005) 143–161, https://doi.org/10.1016/j.chemgeo.2005.03.004.
[40] A. Boubnov, H. Lichtenberg, S. Mangold, J.D. Grunwaldt, Identification of the iron oxidation state and coordination geometry in iron oxide- and zeolite-based catalysts using pre-edge XAS analisis, J. Synchrontron Radiat. 22 (2015) 410–426, https://doi.org/10.1107/S1600577514025880.
[41] M. Yuan, J. Hou, G. Gorni, D. Crespo, Y. Li, T. Pradell, Jun ware glaze colours: an X-ray absorption spectroscopy study, J. Eur. Ceram. Soc. 42 (2022) 3015–3022, https://doi.org/10.1016/j.jeurceramsoc.2022.02.016.
[42] Y. Li, A. Audetat, Partitioning of V, Mn, Co, Ni, Cu, Zn, As, Mo, Ag, Sn, Sb, W, Au, Pb, and Bi between sulfide phases and hydrous basanite melt at upper mantle conditions, Earth Planet Sci. Lett. 355–356 (2012) 327–340, https://doi.org/10.1016/j.epsl.2012.08.008.
[43] E.M. Ripley, J.G. Brophy, C. Li, Copper solubility in a basaltic melt and sulfide liquid/silicate melt partition coefficients of Cu and Fe, Geochem. Cosmochim. Acta 66 (15) (2002) 2791–2800, https://doi.org/10.1016/S0016-7037(02)00872-4.
[44] K.D. Jayasuriya, H. St, C. O'Neill, A.J. Berry, S.J. Campbell, A Mössbauer study of the oxidation state of Fe in silicate melts, Am. Mineral. 89 (2004) 1597–1609, https://doi.org/10.2138/am-2004-11-1203.
[45] M.E. Fleet, Phase equilibria at high temperatures, Rev. Mineral. Geochem. 61 (1) (2006) 365–419, https://doi.org/10.2138/rmg.2006.61.7.
[46] B.J. Skinner, Stability of the tetragonal polymorph of Cu_2S, Econ. Geol. 65 (6) (1970) 724–730, https://doi.org/10.2113/gsecongeo.65.6.724.
[47] T. Machani, D.P. Rossi, B.J. Golden, E.C. Jones, M. Lotfipour, K.E. Plass, Synthesis of monoclinic and tetragonal chalcocite nanoparticles by iron-induced stabilization, Chem. Mater. 23 (2011) 24, https://doi.org/10.1021/cm2022196, 5491−5495.
[48] H.L. Liu, X. Shi, F.F. Xu, L.L. Zhan, W.Q. Zhang, L.D. Chen, Q. Li, C. Uher, T. Day, G.J. Snyder, Copper ion liquid-like thermoelectrics, Nat. Mater. 11 (2012) 422–425, https://doi.org/10.1038/NMAT3273.
[49] P.F. Qiu, X. Shi, L.D. Chen, Thermoelectric properties of $Cu_{2-\delta}X$ (X = S, Se, and Te), in: C. Uher (Ed.), Materials Aspect of Thermoelectricity, CRC Press, Boca Raton, 2016, pp. 289–316, https://doi.org/10.1201/9781315197029.